

# Symplectic Modeling of Beam Loading in Electromagnetic Cavities

Dan T. Abell,\* Nathan M. Cook, and Stephen D. Webb

*RadiaSoft, LLC, 1348 Redwood Ave., Boulder, CO 80304*

(Dated: December 9, 2024)

Simulating beam loading in radiofrequency accelerating structures is critical for understanding higher-order mode effects on beam dynamics, such as beam break-up instability in energy recovery linacs. Full wave simulations of beam loading in radiofrequency structures are computationally expensive, while reduced models can ignore essential physics and can be difficult to generalize. We present a self-consistent algorithm derived from the least-action principle which can model an arbitrary number of cavity eigenmodes and with a generic beam distribution.

## I. INTRODUCTION

The interaction of charged-particle beams and electromagnetic fields drive a variety of applications and phenomena in accelerator systems. These range from klystrons to beam-loading in radiofrequency (RF) cavities to high-order-mode instabilities in energy-recovery linacs. Accurate, self-consistent modeling of these interactions is an important and challenging problem for a number of reasons.

Self-consistent simulations of these systems using approaches such as finite-difference time-domain (FDTD) particle-in-cell (PIC) algorithms [1] are computationally demanding and suffer from a variety of numerical artifacts—for example, the numerical Čerenkov [2] instability, or dispersive errors induced by the mesh [3]—that can muddy the results. Detailed simulations of an electron beam passing through an RF cavity must resolve the current (i.e. the electron beam), and hence require cell dimensions that are small compared to the beam. Resolving the beam across the entire complex geometry can therefore require billions of cells, while the actual source terms are isolated to a mere few thousands of cells. As a consequence, load balancing is a serious concern for multi-core simulations.

The discrepancy of spatial scales is not the only challenge such algorithms face. One must also initialize the fields on the numerical mesh in a manner that satisfies the appropriate numerical dispersion relation. In addition, the presence of multiple bunches means that one must address the discrepancy of temporal scales that effectively prevents using such algorithms to study the effect of high-order modes on beam dynamics.

To bridge multiple scales, one often resorts to reduced models, as, for example, when studying beam loading. Such models typically treat the RF cavity as a thin lens, using reduced forms of the Shockley-Ramo theorem [4, 5] to compute the energy transfer; and they can advance the field phases analytically once the beam passes. Reduced models are computationally much more efficient than full simulations. They also simplify the diagnostics, because the energy in each cavity mode is a dynamical

variable and requires no additional computation to be extracted from the simulation. However, they can fail to demonstrate complicated phase-space structures that result from beam-beam disruption in a collider (as in the eRHIC energy recovery linac-ring design for an electron-ion collider) or from a large energy spread (as results from advanced tapering schemes for free-electron lasers). The approximations made in reduced models frequently do not fail gracefully, and they are difficult to expand to next-leading-order, which can limit their versatility.

What we require is an algorithm that has the simplicity and physically intuitive feel of a reduced model, while being extensible for self-consistent simulations. In this paper, we present such an algorithm based on a symplectic map approach to electromagnetic particle-in-mode algorithms [6]. For this approach we use the cavity eigenmodes as our orthonormal basis for the electromagnetic field. We consider only the coupling of  $j_z$  to  $A_z$ , neglecting the transverse currents. And the modes themselves we compute using either an analytic model or interpolation of numerical data [7]. This approach leads to a fast, extensible model for beam loading with arbitrary numbers of modes and cavity geometries.

## II. THE RATIONALE FOR A SPECTRAL TIME-BASED ALGORITHM

Self-consistent updates of Maxwell's equations require that the fields obey the boundary conditions. For FDTD-type algorithms—the canonical example being the staggered-Yee scheme [8]—this is not difficult: the basis used to decompose the fields is local in space, and it is easy to compute reflections off boundaries, transient effects, etc. FDTD algorithms are also popular for electromagnetics because they can handle complex boundaries, and the electromagnetic part of the algorithm is embarrassingly parallel. However, these algorithms must resolve the smallest features in a simulation, typically the beam itself, and they have inherent dispersive errors that make accurate simulation of beam loading a challenge. Artificial instabilities such as numerical Čerenkov add to the challenge, thus overall making the FDTD approach unsuitable for studying beam loading in most structures.

One possible solution is to use a spectral algorithm that does a global decomposition of the fields as a superposi-

\* [dabell@radiasoft.net](mailto:dabell@radiasoft.net); [www.radiasoft.net](http://www.radiasoft.net)

tion of the cavity eigenmodes. Each mode frequency is known exactly<sup>1</sup>, meaning that in the absence of a source term it is possible to evolve the fields exactly. Adding the source term – the beam – is a convolution integral of the source currents and charges with each field eigenmode. The beam itself takes up a small volume of the simulation domain. Using the field eigenmodes removes the longest length scale from the simulation, dramatically reducing the computational resources required. It also makes source deposition in an electromagnetic simulation embarrassingly parallel, as compared to deposition for FDTD, which can encounter load balancing issues that impede parallel scaling<sup>2</sup>. This can make the spectral approach competitive for performance with FDTD algorithms. Because beam loading requires exact frequency information and field maps to compute properly, and the sources are located on a small fraction of the simulation domain which causes severe load balancing issues for FDTD particle-in-cell simulations, spectral algorithms are ideal for self-consistent beam loading simulations.

Conventional accelerator tracking codes almost universally use the distance along the design orbit of a ring or linac as the independent variable (*s*-based tracking). When including collective effects, there is an issue of simultaneity in the Poisson equation that leads to codes either adopting time as the independent variable (*t*-based tracking) or to use various tricks to make the particle times simultaneous. Single particle integration through standing wave structures, such as radiofrequency cavities, can be accomplished so long as the self-consistent evolution of the fields is neglected.

In a waveguide type structure, which has translational symmetry in the longitudinal direction, *s*- or *t*-based tracking can be used. For systems with *s*-varying transverse geometries, such as RF cavities or traveling wave tubes,

we must use *t*-based tracking. It is easiest to understand this by looking at how an ultra-relativistic beam ( $\beta \approx 1$ ) would affect an *s*- versus *t*-based spectral representation. The fields from the bunch radiate purely transversely, before encountering the cavity surface. If that surface has any tilt to it, the fields reflect off the cavity surface and back into the cavity. In an *s*-based approach, this would produce a local-in-*s* increase in the individual cavity eigenmode strengths on the surface, creating surface currents. These surface currents are not self-consistent with any single eigenmode, so the fields would re-radiate. An *s*-based eigenmode representation has a scattering term between multiple eigenmodes. This is not the case for a *t*-based approach, which changes the eigenmode amplitudes and their associated surface currents by a multiplicative constant, but which are still self-consistent for a single eigenmode.

Simply, an *s*-based algorithm with *s*-varying geometry has scattering terms between the eigenmodes, while a *t*-based algorithm would not. For the problem of a standing wave rf cavity, this means that a *t*-based algorithm is simpler. For a waveguide with no longitudinal variation in the boundaries, either *s*- or *t*-based algorithms can be used.

### III. SELF-CONSISTENT BEAM LOADING ALGORITHM

#### A. Beam Low Lagrangian

We begin with the Low Lagrangian [9] for relativistic particles in electromagnetic fields:

$$\mathcal{L} = \int d\mathbf{x}_0 d\mathbf{v}_0 \left[ -mc^2 \sqrt{1 - \left( \frac{\partial \mathbf{x}}{\partial \tau} \right)^2} - q\phi(\mathbf{x}, t) + q \frac{d\mathbf{x}}{d\tau} \cdot \mathbf{A}(\mathbf{x}, t) \right] \psi(\mathbf{x}_0, \mathbf{v}_0) + \frac{1}{8\pi} \int d\mathbf{x} \left[ \left( -\frac{\partial \mathbf{A}}{\partial \tau} - \nabla \phi \right)^2 - (\nabla \times \mathbf{A})^2 \right]. \quad (1)$$

We use  $\tau = ct$  as our independent variable and Gaussian c.g.s. units throughout.

If we neglect the beam space charge, and consider only the cavity eigenmodes, then  $\phi = 0$ . Furthermore, our

beam has  $|d\mathbf{x}_\perp/d\tau| \ll dz/d\tau \sim 1$ , while  $|\mathbf{A}_\perp| \sim A_z$ . We can therefore neglect the transverse coupling terms. This leaves us with what we call the *beam electromagnetic Low Lagrangian*

$$\mathcal{L} = \int d\mathbf{x}_0 d\mathbf{v}_0 \left[ -mc^2 \sqrt{1 - \left( \frac{\partial \mathbf{x}}{\partial \tau} \right)^2} + q \frac{dz}{d\tau} A_z(\mathbf{x}, t) \right] \psi(\mathbf{x}_0, \mathbf{v}_0) + \frac{1}{8\pi} \int d\mathbf{x} \left[ \left( \frac{\partial \mathbf{A}}{\partial \tau} \right)^2 - (\nabla \times \mathbf{A})^2 \right]. \quad (2)$$

<sup>1</sup> Or to within numerical tolerances, if the fields are solved numerically using a frequency domain solver

<sup>2</sup> It is worth noting that, because spectral algorithms are global instead of local algorithms, they require an `MPI_AllReduce` to

consolidate the source terms. This prevents spectral algorithms from scaling indefinitely, and may require specialized algorithms which reduce the need for many-core simulations at the expense of generality.

This approximation—in essence neglecting  $\mathbf{j}_\perp$ —can be made in the interest of speed, as it dramatically reduces the number of required source depositions, which dominates the computation time for self-consistent simulations.

We assume the cavity eigenmodes are known and form a complete orthonormal basis, so that we may decompose

$$\mathcal{L} = \int d\mathbf{x}_0 d\mathbf{v}_0 \left[ -mc^2 \sqrt{1 - \dot{\mathbf{x}}^2} + q\dot{z} \sum_\ell a_\ell \mathbf{z} \cdot \mathbf{f}_\ell(\mathbf{x}) \right] \psi(\mathbf{x}_0, \mathbf{v}_0) + \frac{1}{8\pi} \sum_\ell \left[ \dot{a}_\ell^2 \int d\mathbf{x} |\mathbf{f}_\ell(\mathbf{x})|^2 - a_\ell^2 \int d\mathbf{x} |\nabla \times \mathbf{f}_\ell(\mathbf{x})|^2 \right], \quad (4)$$

where overdot denotes differentiation with respect to  $\tau$ . As a convenience, we also define the mode inductance  $1/L_\ell = (4\pi)^{-1} \int d\mathbf{x} |\nabla \times \mathbf{f}_\ell|^2$ , and the mode capacitance  $C_\ell = (4\pi)^{-1} \int d\mathbf{x} |\mathbf{f}_\ell(\mathbf{x})|^2$ .

To trace the particles, we introduce macroparticles by decomposing the phase-space density in discrete shapes

$$\mathcal{L} = \sum_{j=1}^{N_{\text{macro}}} \left[ -w_j mc^2 \sqrt{1 - (\dot{\mathbf{x}}^{(j)})^2} + w_j q\dot{z}^{(j)} \sum_\ell a_\ell F_\ell(\mathbf{x}^{(j)}) \right] + \frac{1}{2} \sum_\ell \left[ C_\ell \dot{a}_\ell^2 - \frac{1}{L_\ell} a_\ell^2 \right], \quad (6)$$

where

$$F_\ell(\mathbf{x}^{(j)}) = \mathbf{z} \cdot \int d\mathbf{x} \mathbf{f}_\ell(\mathbf{x}) \Lambda(\mathbf{x} - \mathbf{x}^{(j)}) \quad (7)$$

represents the coupling of particle shape to field shape. Each of the individual  $\mathbf{x}^{(j)}$  and  $a_\ell$  are dynamical variables in this particle-in-mode discrete Lagrangian.

One approach to numerically integrating the resulting equations of motion revolves around using time-discrete Lagrangians [13]. This approach, however, typically yields an implicit algorithm, which is substantially slower than an explicit version. We therefore opt to develop explicit symplectic maps using a canonical formalism.

## B. Particle-Field Hamiltonian and a Split Operator Approach

We can compute the Hamiltonian corresponding to the Lagrangian from the canonical coordinates and conjugate momenta for the particles and fields:

$$\mathbf{q}_j = \mathbf{x}_j, \quad (8a)$$

$$\mathbf{p}_\perp^{(j)} = w_j mc \frac{\dot{\mathbf{x}}_\perp^{(j)}}{\sqrt{1 - (\mathbf{x}^{(j)})^2}}, \quad (8b)$$

the vector potential in these modes:

$$\mathbf{A} = \sum_\ell a_\ell(\tau) \mathbf{f}_\ell(\mathbf{x}), \quad (3)$$

where the  $\mathbf{f}_\ell$  denote spatial eigenmodes, and  $a_\ell$  the corresponding mode amplitudes. Plugging this form into the Low Lagrangian, we obtain

in the usual manner [6, 10–12]:

$$\psi(\mathbf{x}, \dot{\mathbf{x}}) = \sum_{j=1}^{N_{\text{macro}}} w_j \Lambda(\mathbf{x} - \mathbf{x}^{(j)}) \delta(\dot{\mathbf{x}} - \dot{\mathbf{x}}^{(j)}). \quad (5)$$

Here  $w_j$  denote the macroparticle weights,  $\delta$  the Dirac delta function, and  $\Lambda$  the normalized particle shape functions (so that  $\int d\mathbf{x} \Lambda = 1$ ). This decomposition transforms the Lagrangian (4) into a discrete set of coupled macroparticle-electromagnetic-mode Lagrangians:

$$\mathbf{p}_z^{(j)} = w_j mc \frac{\dot{z}^{(j)}}{\sqrt{1 - (\mathbf{x}^{(j)})^2}} - w_j qA_z, \quad (8c)$$

$$Q_\ell = a_\ell, \quad (8d)$$

$$P_\ell = C_\ell \dot{a}_\ell. \quad (8e)$$

The particle conjugate momenta are the usual, but with the  $\mathbf{A}_\perp$  components neglected. The field conjugate momentum includes the mode capacitance, which acts like an effective mass for the mode.

The Legendre transform to compute the coupled particle-field Hamiltonian is

$$\mathcal{H} = \sum_j c \mathbf{p}_j \cdot \dot{\mathbf{q}}_j + \sum_\ell c P_\ell \dot{Q}_\ell - \mathcal{L}. \quad (9)$$

Carrying out this Legendre transform for these variables yields the particle-field Hamiltonian

$$\mathcal{H} = \sum_j c \underbrace{\sqrt{\left(\mathbf{p}_\perp^{(j)}\right)^2 + \left(p_z^{(j)} - w_j \frac{q}{c} \sum_\ell Q_\ell F_\ell(\mathbf{q}^{(j)})\right)^2 + w_j^2 m^2 c^2}}_{\mathcal{H}_{\text{p-c}}} + \underbrace{\frac{1}{2} \sum_\ell \left[\frac{P_\ell^2}{C_\ell} + \frac{1}{L_\ell} Q_\ell^2\right]}_{\mathcal{H}_{\text{f}}}, \quad (10)$$

where  $\mathcal{H}_{\text{p-c}}$  denotes the particle-coupling Hamiltonian, and  $\mathcal{H}_{\text{f}}$  denotes the field Hamiltonian.

The mode quantities  $C_\ell$  and  $L_\ell$  are determined only up to within a normalization constant. This means that the individual definitions of  $Q_\ell$  and  $P_\ell$  will depend on the normalization convention used for  $\mathbf{f}_\ell$ . It will prove useful to make a canonical transformation that combines the two into a single scale-invariant quantity, which would be an intrinsic quantity for a given cavity eigenmode.

By defining the canonically conjugate variables

$$Q_\ell = \sqrt{C_\ell} Q_\ell, \quad (11a)$$

$$\mathcal{P}_\ell = \sqrt{\frac{1}{C_\ell}} P_\ell, \quad (11b)$$

we transform the field and particle-coupling Hamiltonians into

$$\mathcal{H}_{\text{f}} = \frac{1}{2} \sum_\ell \left[ \mathcal{P}_\ell^2 + \frac{1}{L_\ell C_\ell} Q_\ell^2 \right] \quad (12a)$$

and

$$\begin{aligned} \mathcal{H}_{\text{p-c}} &= c \sum_j \left[ \left(\mathbf{p}_\perp^{(j)}\right)^2 \right. \\ &\quad \left. + \left(p_z^{(j)} - w_j \frac{q}{c} \sum_\ell Q_\ell \frac{1}{\sqrt{C_\ell}} F_\ell(\mathbf{q}^{(j)})\right)^2 + w_j^2 m^2 c^2 \right]^{1/2} \end{aligned} \quad (12b)$$

All quantities in these Hamiltonians—including  $Q_\ell$ ,  $\mathcal{P}_\ell$ , and  $F_\ell/\sqrt{C_\ell}$ —are independent of our choice of normalization for  $\mathbf{f}_\ell$ . The invariant combination of the mode capacitance and inductance is

$$\Omega_\ell^2 = \frac{1}{L_\ell C_\ell} = \frac{\int d\mathbf{x} |\nabla \times \mathbf{f}_\ell(\mathbf{x})|^2}{\int d\mathbf{x} |\mathbf{f}_\ell(\mathbf{x})|^2}, \quad (13)$$

which yields the eigenmode frequency,  $\Omega_\ell$ .

### C. Splitting the Hamiltonian

The total particle-field Hamiltonian has no explicit time dependence, so the symplectic map [14–16] for going from time  $\tau$  to time  $\tau + h$  is simply

$$\mathcal{M}(\tau \rightarrow \tau + h) = \exp(-:\mathcal{H}_{\text{p-c}} + \mathcal{H}_{\text{f}}: h). \quad (14)$$

This map may be split symmetrically into a map which is second-order accurate in  $h$ :

$$\mathcal{M}(h) \approx \mathcal{M}_{\text{f}}^{(h/2)} \mathcal{M}_{\text{p-c}}(h) \mathcal{M}_{\text{f}}^{(h/2)}, \quad (15a)$$

where

$$\mathcal{M}_{\text{f}}^{(h/2)} = \exp\left(-:\mathcal{H}_{\text{f}}: \frac{h}{2}\right), \quad (15b)$$

$$\mathcal{M}_{\text{p-c}}(h) = \exp(-:\mathcal{H}_{\text{p-c}}: h), \quad (15c)$$

and all maps are independent of the initial time  $\tau$ . We can evaluate both  $\mathcal{M}_{\text{f}}$  and  $\mathcal{M}_{\text{p-c}}$  to second order in  $h$ , leading to a second-order symplectic integrator for both the fields and the particles.

#### 1. Field Map

The field map  $\mathcal{M}_{\text{f}}$ , is simply the harmonic oscillator, and it acts only on the field phase-space coördinates:

$$\begin{aligned} \begin{pmatrix} Q_\ell \\ \mathcal{P}_\ell \end{pmatrix}_{\text{fin}} &= \mathcal{M}_{\text{f}}^{(h/2)} \circ \begin{pmatrix} Q_\ell \\ \mathcal{P}_\ell \end{pmatrix}_{\text{ini}} \\ &= \begin{pmatrix} \cos(\Omega_\ell \frac{h}{2}) & \Omega_\ell^{-1} \sin(\Omega_\ell \frac{h}{2}) \\ -\Omega_\ell \sin(\Omega_\ell \frac{h}{2}) & \cos(\Omega_\ell \frac{h}{2}) \end{pmatrix} \begin{pmatrix} Q_\ell \\ \mathcal{P}_\ell \end{pmatrix}_{\text{ini}} \end{aligned} \quad (16)$$

As is usually the case with second-order splitting, the two half-step field maps can, for simplicity, be combined into a single full-step map—so long as one retains the half-step maps at the *ends* of the simulation.

#### 2. Particle-Coupling Map

The particle-coupling map is not immediately integrable, but it can be split using a method described by Wu, Forest, and Robin [17] and exploited by Webb *et al.* [6] for a cylindrical electromagnetic algorithm. This method involves tracking each particle with respect to its own proper time, which allows us to re-write the Hamiltonian as an effectively non-relativistic Hamiltonian given by

$$\mathcal{H}_{\text{p-c}} = \sum_j \frac{\left(\mathbf{p}_\perp^{(j)}\right)^2 + \left(p_z^{(j)} - w_j \frac{q}{c} \sum_\ell Q_\ell \frac{1}{\sqrt{C_\ell}} F_\ell(\mathbf{q}^{(j)})\right)^2}{2 w_j m \gamma^{(j)}}, \quad (17)$$

where  $\gamma^{(j)}$  denotes the Lorentz gamma of each macroparticle:

$$\begin{aligned} \gamma^{(j)} w_j m c^2 = c \left[ \left( \mathbf{p}_\perp^{(j)} \right)^2 \right. \\ \left. + \left( p_z^{(j)} - w_j \frac{q}{c} \sum_\ell \mathcal{Q}_\ell \frac{1}{\sqrt{C_\ell}} F_\ell \left( \mathbf{q}^{(j)} \right) \right)^2 + w_j^2 m^2 c^2 \right]^{1/2} \end{aligned} \quad (18)$$

$$\mathcal{M}_{\text{p-c}} \approx \exp \left[ - \sum_j : \frac{\left( \mathbf{p}_\perp^{(j)} \right)^2}{2 w_j m \gamma^{(j)}} : \frac{h}{2} \right] \exp \left[ - \sum_j : \frac{\left( p_z^{(j)} - w_j \frac{q}{c} \sum_\ell \mathcal{Q}_\ell \frac{1}{\sqrt{C_\ell}} F_\ell \left( \mathbf{q}^{(j)} \right) \right)^2}{2 w_j m \gamma^{(j)}} : h \right] \exp \left[ - \sum_j : \frac{\left( \mathbf{p}_\perp^{(j)} \right)^2}{2 w_j m \gamma^{(j)}} : \frac{h}{2} \right]. \quad (19)$$

This result is again second-order accurate in  $h$  and hence preserves the overall order of the integrator.

The drift maps are particularly simple:

$$\begin{aligned} \exp \left[ - \sum_j : \frac{\left( \mathbf{p}_\perp^{(j)} \right)^2}{2 w_j m \gamma^{(j)}} : \frac{h}{2} \right] \circ \left( \begin{array}{c} \mathbf{p}_\perp^{(j)} \\ \mathbf{q}_\perp^{(j)} \end{array} \right)_{\text{ini}} = \\ \left( \begin{array}{c} \mathbf{p}_\perp^{(j)} \\ \mathbf{q}_\perp^{(j)} + h \mathbf{p}_\perp^{(j)} / w_j m \gamma^{(j)} \end{array} \right)_{\text{ini}}. \end{aligned} \quad (20)$$

We can now apply the technique in [17] to deal with the vector potential. Lie transformations obey an important similarity transformation property:

$$e^{f:} e^{g:} e^{-f:} = e^{e^{f:} g:}. \quad (21)$$

This property allows us to rewrite the middle map in (19) as the product of three maps:

$$\begin{aligned} \exp \left[ - \sum_j : \frac{\left( p_z^{(j)} - w_j \frac{q}{c} \sum_\ell \mathcal{Q}_\ell \frac{1}{\sqrt{C_\ell}} F_\ell \left( \mathbf{q}^{(j)} \right) \right)^2}{2 w_j m \gamma^{(j)}} : h \right] = \\ \underbrace{\exp \left[ - \sum_j \sum_\ell w_j \frac{q}{c} : \mathcal{Q}_\ell \frac{1}{\sqrt{C_\ell}} \int dz F_\ell \left( \mathbf{q}^{(j)} \right) : \right]}_{\mathcal{A}_z} \times \\ \underbrace{\exp \left[ - \sum_j : \frac{\left( p_z^{(j)} \right)^2}{2 w_j m \gamma^{(j)}} : h \right]}_{\mathcal{D}_z} \times \\ \underbrace{\exp \left[ \sum_j \sum_\ell w_j \frac{q}{c} : \mathcal{Q}_\ell \frac{1}{\sqrt{C_\ell}} \int dz F_\ell \left( \mathbf{q}^{(j)} \right) : \right]}_{\mathcal{A}_z^{-1}}. \end{aligned} \quad (22)$$

Because the vector potential has no *explicit* time dependence,  $\gamma^{(j)}$  is a constant of the motion for this Hamiltonian, and the proper time of each macroparticle can be mapped to the lab time simply by multiplying by  $\gamma^{(j)}$ . Once written in the form (17), the Hamiltonian can be split and integrated using a drift map for the transverse coordinates, and another map for the  $z$ -coordinate:

Moreover, each of these maps—the drift  $\mathcal{D}_z$  and the transformation  $\mathcal{A}_z$ —can be evaluated exactly:

$$\mathcal{D}_z \circ \left( \begin{array}{c} p_z^{(j)} \\ z^{(j)} \end{array} \right) = \left( \begin{array}{c} p_z^{(j)} \\ z^{(j)} + \frac{p_z^{(j)}}{w_j m \gamma^{(j)}} h \end{array} \right) \quad (23a)$$

$$\begin{aligned} \mathcal{A}_z \circ \left( \begin{array}{c} \mathcal{P}_\ell \\ \mathcal{Q}_\ell \end{array} \right) = \\ \left( \begin{array}{c} \mathcal{P}_\ell + \sum_j w_j \frac{q}{c} (\sqrt{C_\ell})^{-1} \int dz F_\ell \left( \mathbf{q}^{(j)} \right) \\ \mathcal{Q}_\ell \end{array} \right) \end{aligned} \quad (23b)$$

$$\begin{aligned} \mathcal{A}_z \circ \left( \begin{array}{c} \mathbf{p}_\perp^{(j)} \\ \mathbf{q}_\perp^{(j)} \end{array} \right) = \\ \left( \begin{array}{c} \mathbf{p}_\perp^{(j)} + \nabla_{\mathbf{q}} \sum_\ell w_j \frac{q}{c} (\sqrt{C_\ell})^{-1} \mathcal{Q}_\ell \int dz F_\ell \left( \mathbf{q}^{(j)} \right) \\ z^{(j)} \end{array} \right) \end{aligned} \quad (23c)$$

Because the algorithm is based on explicit symplectic maps, it is possible to implement each of these maps as a single function, and the update sequence is just a series of function calls. Once each of these maps is implemented, it is straightforward to begin simulations.

#### IV. NUMERICAL RESULTS

To test the algorithm described in this paper, we considered a number of configurations to test energy conservation. In all tests, we considered a rectangular pillbox cavity with a handful of test macroparticles. We list the specific parameters in table I. In all simulations we considered four cavity modes: an accelerating mode, two transverse dipole modes, and a single transverse quadrupole mode.

A high bunch charge was selected to demonstrate the field energy loss—otherwise the total energy of the bunch is so much smaller than the total energy in the fields that the variations are not easy to discern.

Parameter	Quantity
Bunch Charge	192 nC
$e$ -beam Energy	25.5 MeV
Total Bunch Energy	$4.8 \times 10^7$ ergs
Accelerating Gradient	5.1 MV/m
Cavity Length	10 cm
Cavity Width $\times$ Cavity Height	50 cm $\times$ 40 cm
Fundamental Frequency	$2\pi \times 959$ MHz

TABLE I. Simulation parameters for testing the algorithm.

In the first test, we considered a configuration with a single macroparticle representing the entire bunch, accelerated from  $\gamma = 50$  to  $\gamma = 51$ . The particle is on-axis, so no higher order modes should be excited. The result is shown in figure 1. As can be seen, the energy conservation is excellent, and none of the higher order modes are excited.

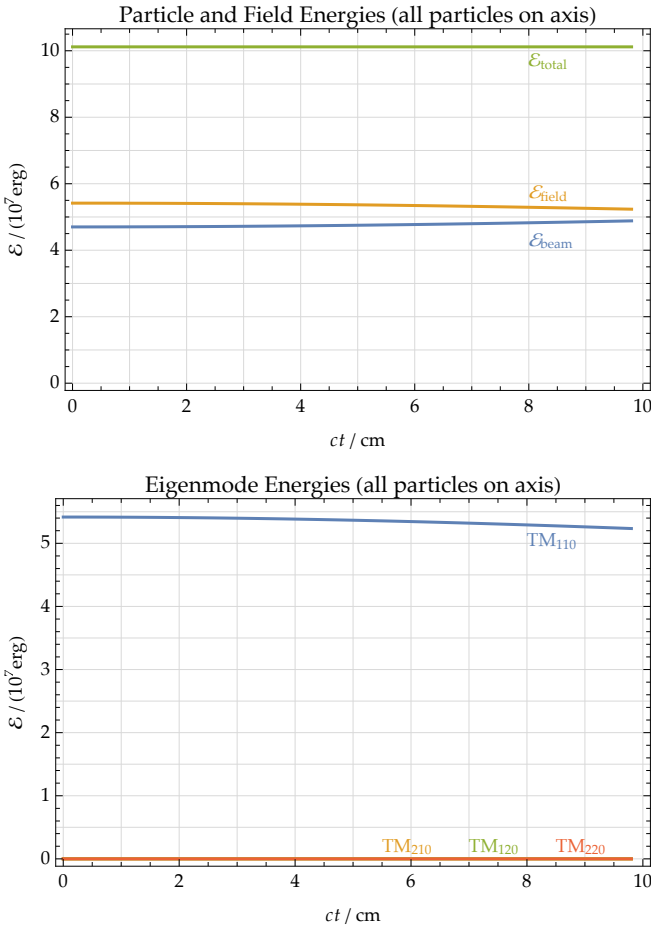


FIG. 1. Energy gain and eigenmode energy decomposition for a single on-axis particle.

To test the excitation of higher order modes, we split the beam into four macroparticles—one on-axis; one offset in  $x$  and another offset in  $y$  to excite dipole modes; and one offset along the  $x$ - $y$  diagonal to excite both dipole

and quadrupole modes. As shown in figure 2, the total

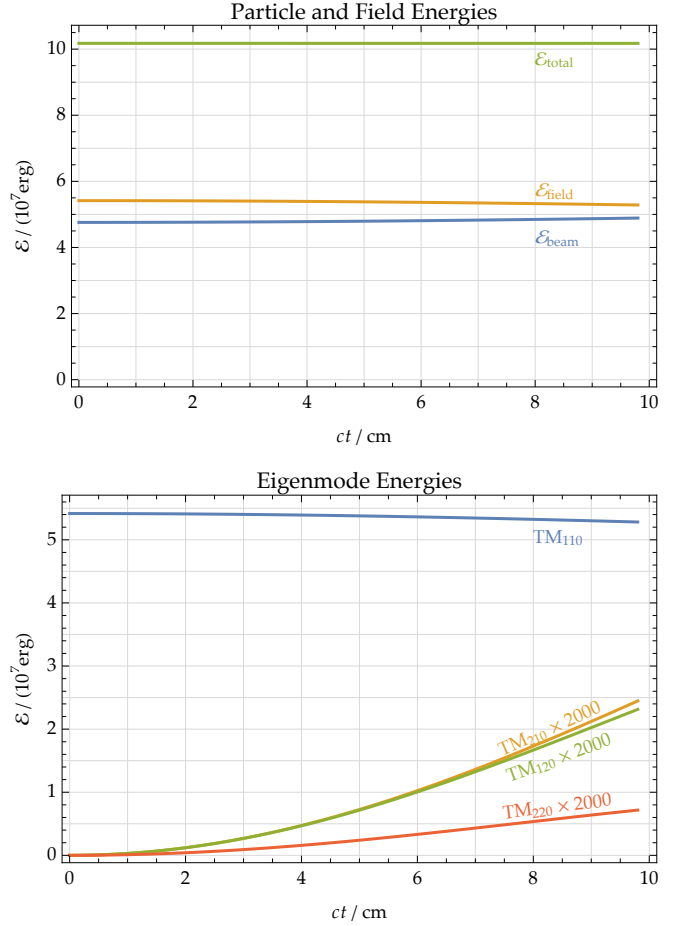


FIG. 2. Total particle-field energy and individual mode energies for the four-particle configuration.

energy is conserved to high precision, and all the modes are excited, although the fundamental mode sees the most variation.

Because this is a symplectic integrator, we expect the total energy to be well-behaved for arbitrarily long time. To test this, we considered a much longer rectangular pillbox, 125 cm long, with the same transverse eigenmodes. As shown in figure 3, the algorithm retains stable energy behavior for longer time scales. This captures oscillatory behavior as the beam accelerates and decelerates, and the particles slip in phase for the higher order modes.

When simulating considerably longer cavities,  $> 4000$  cm in length, we detected a slow spurious decay in the total energy. Over this length, the error was  $< 0.1\%$  total. We have identified the origin of this spurious decay as numerical roundoff error in the field rotation matrix: for our implementation, the floating-point value of the determinant was very slightly less than 1. Over many time steps this can lead, depending on the roundoff error, to spurious cooling or heating of the system; but for a single bunch pass this is almost undetectable. Furthermore, when advancing the fields in between bunch passes,

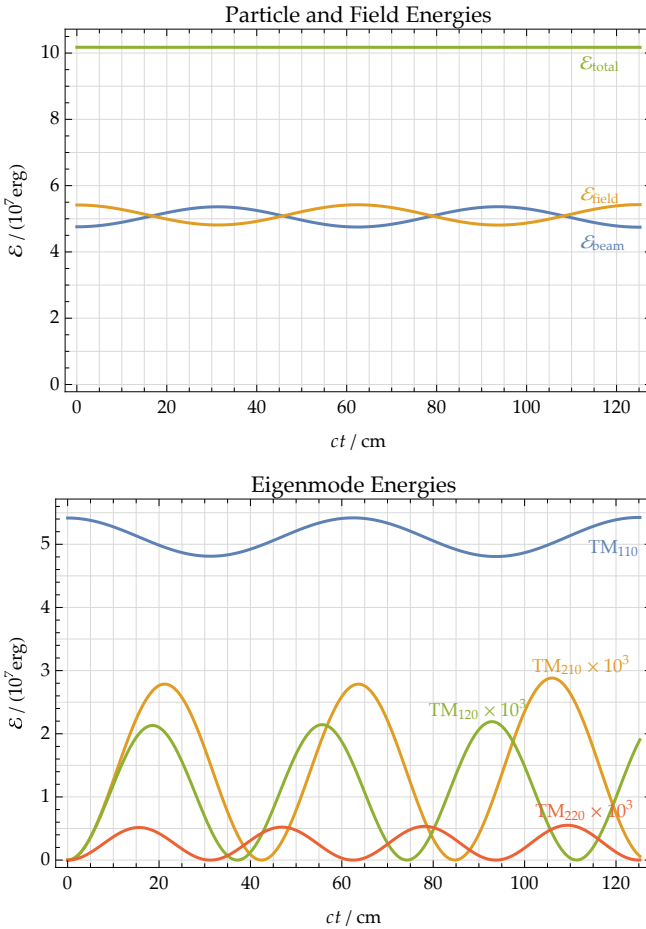


FIG. 3. Total particle-field energy and individual mode energies for the four-particle configuration in a longer cavity.

it suffices to perform a single matrix multiplication to advance the eigenmodes. Doing this reduces the roundoff-induced energy change in multi-bunch and multi-pass simulations performed when studying, for example, energy-recovery linacs.

## V. CONCLUSIONS

We have presented a new approach to simulating beam loading in electromagnetic cavities. The approach is based on a particle-in-mode symplectic map approach to electromagnetic charged-particle simulations. The algorithm

is suitable for modeling a variety of vacuum electronic devices, including radiofrequency cavities, traveling wave tubes, and klystrons.

The algorithm avoids the various pitfalls of both the finite-difference time-domain electromagnetic particle-in-cell and the reduced-model approaches that are typically applied to this problem.

Because the algorithm is directly spectral, there are no grid aliasing artifacts that can result in the numerical instabilities and dispersive errors that tend to infect the full electromagnetic PIC simulations. By using a modal decomposition, it is straightforward to identify, directly from the dynamical data, which cavity eigenmodes are excited and how they evolve—there is no need for post-processing of the simulation data to extract the eigenmodes. The approach also solves the load balancing problem, as the field data is global, and the particles can be evenly distributed across multiple processors. The approach is also much faster than the full self-consistent approach: our simulations of the single particle traversing the pillbox cavity, including generating the figures, required less than a second using an implementation that performed symbolic mathematical computations and is far from optimized.

The symplectic particle-in-mode (SymPIM) algorithm described in this paper in many ways resembles the reduced models, but it is distinct in a number of important ways. Because the cavity is not treated as a thin element, it is possible to model the complex phase-space of realistic beams, such as those with large energy spreads, or those disrupted by beam-beam collisions or various wakefield instabilities.

The SymPIM algorithm thus lies between the fully self-consistent approach—which includes all resolvable cavity modes at great computational expense—and the reduced-model approach—which neglects many details of the beam distribution and how it evolves within the cavity. This makes the SymPIM algorithm suitable for determining the validity of reduced models, as well as for modeling those cases where the reduced models do not apply.

## VI. ACKNOWLEDGEMENTS

This material is based upon work supported by the U.S. Department of Energy, Office of Science, Office of Nuclear Physics under Award Number DE-SC0015211.

---

[1] C. K. Birdsall and A. B. Langdon, *Plasma Physics via Computer Simulation* (McGraw-Hill, New York, 1985).  
[2] Brendan B. Godfrey, “Numerical Cherenkov instabilities in electromagnetic particle codes,” *J. Comp. Phys.* **15**, 504–521 (1975).  
[3] Allen Tafove and Susan C. Hagness, *Computational Electrodynamics*, 2nd ed. (Artech House, 2000).  
[4] W. Shockley, “Currents to Conductors Induced by a Moving Point Charge,” *J. App. Phys.* **9**, 635 (1938).  
[5] S. Ramo, “Currents Induced by Electron Motion,” in *Proceedings of the IRE*, Vol. 27 (1939) pp. 584–584.  
[6] S. D. Webb, D. T. Abell, N. M. Cook, and D. L. Bruhwiler, “A Spectral Symplectic Algorithm for Cylindrical Electromagnetic Plasma Simulations,” ArXiv e-prints (2016),

submitted for publication.

- [7] Dan T. Abell, “Numerical computation of high-order transfer maps for rf cavities,” *Phys. Rev. ST Accel. Beams* **9**, 052001 (2006).
- [8] Kane S. Yee, “Numerical solution of initial boundary value problems involving maxwell’s equations in isotropic media,” *IEEE Trans. Ant. and Prop.* **14**, 302–307 (1966).
- [9] F. E. Low, “A Lagrangian Formulation of the Boltzmann-Vlasov Equation for Plasmas,” *Proc. R. Soc. London Ser. A. Math. Phys. Sci.* **248**, 282–287 (1958).
- [10] A. Stamm, B. Shadwick, and E. Evstatiev, “Variational Formulation of Macro-Particle Models for Electromagnetic Plasma Simulations,” *IEEE Trans. Plasma Science* **42** (2014).
- [11] B. Shadwick, A. Stamm, and E. Evstatiev, “Variational formulation of macro-particle plasma simulation algorithms,” *Phys. Plasmas* **21** (2014).
- [12] Stephen D. Webb, “A Spectral Canonical Electrostatic Algorithm,” *Plasma Phys. Controlled Fusion* **58** (2016).
- [13] J. E. Marsden and M. West, “Discrete Mechanics and Variational Integrators,” *Acta Numerica* , 357–514 (2001).
- [14] A. Dragt and J. Finn, “Lie series and invariant functions for analytic symplectic maps,” *J. Math. Phys.* **17**, 2215–2227.
- [15] Alex J. Dragt, “Lectures on nonlinear orbit dynamics,” in *Physics of High Energy Particle Accelerators*, Vol. 87 (AIP Publishing, 1982) pp. 147–313.
- [16] A. Dragt, *Lie Methods for Nonlinear Dynamics with Applications to Accelerator Physics* (University of Maryland) <http://www.physics.umd.edu/dsat/>.
- [17] Y. K. Wu, É. Forest, and D. S. Robin, “Explicit symplectic integrator for  $s$ -dependent static magnetic fields,” *Phys. Rev. E* **68**, 046502 (2003).